Meteorol Atmos Phys (2011) 114:17–34
DOI 10.1007/s00703-011-0154-8

ORIGINAL PAPER

Influence of convective adjustment time scale on the tropical transient activity

Saroj K. Mishra

Received: 16 July 2011 / Accepted: 25 July 2011 / Published online: 17 August 2011

Abstract The influence of convective adjustment time scale (τ) in simulating the tropical transient activity is examined using the NCAR-Community Atmosphere Model (CAM). In the default configuration of the model, the prescribed value of τ, a characteristic time scale with which convective available potential energy (CAPE) is removed at an exponential rate by convection, is assumed to be 1 h. However, some recent observational findings suggest that it is larger by around one order of magnitude, and subsequent modeling studies showed its impact on mean climate and suggest a value of 8 h. To see if alteration of this time scale could affect the transient features of climate, numerical experiments are conducted in aqua-planet and real-planet frameworks. The analysis includes the tropical intraseasonal variability (ISV), convectively coupled equatorial waves (CCEW), diurnal and sub-diurnal variability of precipitation, and intensity and frequency of rainfall. Two sets of simulations are conducted: one with a time scale of 1 h (CTRL) and another with 8 h (EXPT). EXPT produces more reasonable ISV, with prominent, coherent, and organized eastward propagation. The active phases of the ISV constitute hierarchical substructures embedded within them, which are absent in CTRL. The Kelvin waves become slow, Madden–Julian oscillation (MJO) become energetic, $n = 1$ equatorial Rossby (ER) and $n = 0$ eastward inertio-gravity (EIG) waves become prominent, with the increase of τ. On the contrary, the mixed Rossby-gravity (MRG) waves at higher wavenumber regimes become weak. The amplitude of diurnal variability decreases, but the phase remains largely unchanged. At sub-diurnal scales, the variability of precipitation increases. In CTRL, precipitation always occurs in the tropics with light or moderate intensity, which becomes intermittent when τ is increased to 8 h.

Responsible editor: M. Kaplan.

S. K. Mishra (✉)
Institute for Mathematics Applied to Geosciences (IMAGe),
National Center for Atmospheric Research (NCAR),
1850, Table Mesa Drive, Boulder, CO 80305, USA
e-mail: saroj@ucar.edu

S. K. Mishra
Department of Computer Science, University of Colorado,
Boulder, CO, USA

1 Introduction

Cumulus convection plays a central role in the maintenance and evolution of the tropical atmosphere. The scale of cumulus convection is usually smaller than the typical grid size ($\sim$100–300 km) used in current general circulation models (GCMs) and hence, implicitly represented by parameterizations. There are several tunable parameters used in the cumulus parameterization. Some of the parameters are observable (e.g., particle size distribution), while many are not (e.g., convective adjustment time scale). The selection of suitable values for these unobservable parameters is one of the most challenging tasks. Since these parameters are free and tunable, their values are deduced by an indirect method. The usual method followed is to find the effect of a parameter on the model simulation, and then choose a value, which maximizes agreement with observations (Mapes 2001). These parameters are considered as the weakest link in the chain of the parameterization.

Convection occurs only when there is convective available potential energy (CAPE), which is subsequently removed by sub-grid scale convection at an exponential

rate using an adjustment timescale in NCAR-CAM. The adjustment time scale (τ) determines the intensity and duration of convection for a given CAPE. With small τ the convection is short-lived but the intensity is high, on the other hand with larger τ the convection is long-lived but of low intensity. Secondly, τ determines the lag of the convective response to large-scale forcing. With small τ the model adjusts rapidly toward the stable state, while with larger τ, the model atmosphere moves in the direction of the large-scale forcing. A detail description of τ is presented in Sect. 3.

It was a long-standing belief that τ is about 1–2 h. Betts and Miller (1986) used a single column model and showed that, when the value of τ was set to approximately 2 h, the observed features (e.g., wave structure and amplitude observed during the GATE experiment) were accurately reproduced. Following Betts and Miller (1986), the value of τ has been used as approximately 1–2 h(s) in most of the present day GCMs. The standard value of τ in NCAR-CAM is 1 h, which uses the Zhang–McFarlane (ZM) convection scheme (Collins et al. 2004). In Canadian Center for Climate Modeling and Analysis (CCCma) AGCM3, τ is set to 40 min, which also uses the ZM scheme (Lorant et al. 2006). Recently, Bretherton et al. (2004) have shown from observations that the adjustment time scale is larger by around one order of magnitude than the typical values used in current GCMs. They used SSM/I microwave radiometer data, analyzed the relationship between water vapor path and surface precipitation over the tropical ocean, and discussed about the adjustment time scale. Mishra and Srinivasan (2010) examined the performance of CAM using a variety of time scales ranging from 1 h to infinity and showed that when τ increases, rate of deep convective precipitation (DCP) decreases accompanied with an increase in shallow convective precipitation (SCP) and large-scale precipitation (LSP). The total precipitation (TP) remains approximately the same, but the proportion of the three components changes significantly, which in turn alters the vertical distribution of precipitation. When τ increases, the vertical structure of moist heating changes from a vertically extended profile to a bottom heavy profile, which shifts the altitude of the maximum vertical velocity from upper troposphere to lower troposphere. They showed that in many respects, performance of the model with an 8-h time scale is better than the default settings. Lee et al. (2009) also showed that τ has significant impact in NCAR-CAM2. When they increased τ from 2 to 8 h, there was an improvement in the simulation of water vapor isotope. The previous work suggests using 8 h; however, they did not address its impact on transient features of the climate. Since the transient climatic features are sensitive to model time step (Mishra and Sahany 2011a), it is thought that the convective time scale may have impact on the tropical transient activities, especially in the tropics where convection is one of the most important forcing. As the transient activity occurs in a wide range of spatial and temporal scales and governs the day-to-day weather and short-term climatic condition, it is desirable to understand the influence of the convective time scale on the transient activity, which is the objective of this paper.

The paper is organized as follows. In Sect. 2 the model and numerical experiments are described followed by the role of convective adjustment time scale in cumulus parameterization in Sect. 3. In Sect. 4 the results are presented. This includes the effect of this time scale on the tropical intraseasonal variability (ISV), convectively coupled equatorial waves (CCEW), diurnal and sub-diurnal variability of precipitation, and intensity and frequency of rainfall. Finally summary and discussions are given in Sect. 5.

2 Description of the model and experiments

2.1 Model details

The numerical model used in this study is Community Atmosphere Model version 3 (CAM3), an atmospheric general circulation model (AGCM) developed by NCAR in collaboration with the atmospheric modeling community. The source code, documentation and input datasets for the model were obtained from the CAM website (http://www.ccsm.ucar.edu/models/atm-cam).

CAM3 is designed to produce simulations with reasonable accuracy for various dynamical cores and horizontal resolutions (Collins et al. 2004, 2006). For this study, semi-Lagrangian dynamical (SLD) core was used at 128 × 64 (2.8°) horizontal resolution, 60 min of temporal resolution, and 26 vertical levels. The model uses the hybrid vertical coordinate, which is terrain following at earth's surface, but reduces to pressure coordinate at higher levels near the tropopause.

The moist precipitation consists of deep convective, shallow convective, and stratiform processes. The physical parameterization schemes include Zhang and McFarlane (1995) for deep convective, Hack (1994) for shallow convective and Rasch and Kristjansson (1998) for stratiform precipitation. The updraft ensembles in Zhang and McFarlane scheme are deep penetrative in nature, which rooted in the planetary boundary layer and penetrate into the upper troposphere until their neutral buoyancy levels. The top of the "shallowest" of the convective plumes is assumed to be no lower than the height of the minimum in saturated moist static energy (typically in the mid-troposphere). On the contrary, Hack scheme uses a simple cloud

model based on triplets, in which convective instability is assessed for three adjacent layers in the vertical. If a parcel of air in the lower layer is more buoyant than one in the middle layer, adjustment occurs. So, unlike the deep penetrative plume of Zhang and McFarlane scheme, Hack scheme can have both shallow and deep plumes, but no plume in Hack scheme is deeper than the thickness of 3-model layers. Secondly, in the tropical atmosphere the typical moist static energy has its minima in the mid-troposphere, so the triplet cloud model mainly works in the lower and middle troposphere. The above-discussed designed principle of Hack scheme is such, even when Zhang and McFarlane scheme is inactive/absent (i.e. where only Hack scheme was operating) it could not produce plumes, which are deeper than 3-model layers. So, it is more like a local scheme that primarily does shallow and mid-level convection.

Separate prognostic equations have been included for the liquid and ice-phase condensate. Condensed water detrained from shallow and frontal convection can form either precipitation or additional stratiform cloud water. Convective precipitation can evaporate into its environment at a rate determined by Sundqvist (1988). Equations governing cloud condensate include advection and sedimentation of cloud droplets and ice particles. The settling velocities for liquid and ice-phase constituents are computed separately as functions of particle size characterized by the effective radius. Small ice particles are assumed to fall like spheres according to the Stokes equation. With the increase in size of the ice particles, there is a smooth transition to a different formulation for fall speeds following Locatelli and Hobbs (1974). In the case of liquid drops, fall velocities are calculated using Stokes equation for the entire range of sizes.

To ensure conservation of energy (Boville and Bretherton 2003), the calculation of thermodynamic tendencies was reformulated. The dry static energy is predicted by each physical parameterization and is immediately updated. Temperature and geopotential are then obtained from the updated value of dry static energy. The dissipation of kinetic energy from vertical diffusion of momentum is calculated explicitly and included in the heating applied to the atmosphere.

2.2 Experiments details

For this work, we carried out two sets of numerical experiments, one in an aqua-planet framework and the other in a real-planet framework. Since aqua-planet framework is relatively simpler in comparison to real-planet framework, understanding of the underlying mechanism is often easier. Finally, to see how the aqua-planet results translate to full AGCM, integrations were performed in real-planet framework.

In the aqua-planet configuration all the land points are replaced by ocean points such that the surface drag coefficients, albedo, and evaporation characteristics are homogeneous over the globe. A further simplification was obtained by fixing the solar declination. Solar insolation was fixed to be same as on 21 March, which puts the sun overhead at the equator. Additionally this produces another desirable simplification by providing approximate hemispheric symmetry of insolation forcing. The experiments have been performed with a zonally symmetric sea surface temperatures (SST) profile as boundary condition. The distribution of SST used in the simulation is similar to the control SST of Neale and Hoskins (2000). Two simulations were performed, one with $\tau = 1$ h (CTRL) and another with $\tau = 8$ h (EXPT). The initial condition for both simulations was from a previous aqua-planet simulation. All the integrations were performed for 18 months and the last 12 months were used for analysis. It is believed that 18 months is long enough for aqua-planet study (Mishra et al. 2008; Williamson 2008; Mishra and Sahany 2011a, 2011b). Additional numerical experiments were performed for sensitivity studies, which will be explained in the text in the respective places.

In real-planet framework, two 10-year (January 1979–December 1988) simulations were performed, one with $\tau = 1$ h and another with $\tau = 8$ h. This framework uses actual land–ocean distribution with topography, observed sea surface temperature (Rayner et al. 2003) and seasonal cycle of solar radiation. The initial condition used was generated for 1 Jan. 1979. Soil moisture and snow cover were computed by the model.

3 Role of convective adjustment time scale in the convective parameterization

The closure for the ZM scheme is based on the budget equation for CAPE. This budget equation may be written as:

$$\partial A/\partial t = -M_{\mathrm{b}}F + G \tag{1}$$

where, A represents CAPE, G represents the large-scale production of CAPE by the grid scale dynamics, and $-M_{\mathrm{b}}F$ represents the sub-grid scale CAPE consumption by the parameterized deep convection. M_{b} represents the cloud base mass flux, and F represents the rate at which cumulus clouds consume CAPE per unit cloud base mass flux. The closure used in the scheme is a diagnostic closure condition in CAM3, which is as follows:

$$M_b = A/\tau F \quad (2)$$

where, τ is the convective adjustment time scale. This closure assumes that CAPE is consumed at an exponential rate ($1/\tau$) by cumulus convection. This may be seen by substituting eq. 2 in eq. 1, which will give eq. 3.

$$\partial A/\partial t = -A/\tau + G. \quad (3)$$

So, if CAPE is A_0 at $t = 0$, in the absence of large-scale CAPE generation, the solution will be $A = A_0 \exp(-t/\tau)$, for $t > 0$. Hence, when the adjustment time scale is increased, it will reduce the magnitude of cloud base mass flux. This in turn determines the updraft mass flux at every level of the model, by taking the entrainment and detrainment rate into consideration. Eventually, updraft mass flux along with cloud liquid water determines the deep convective precipitation (DCP) production at every model level, as in eq. 4.

$$[\mathrm{DCP}]_i = \mathrm{C0} \times [M_u]_i [L]_i \quad (4)$$

where, C0 is the DCP production efficiency parameter, M_u is the updraft mass flux, and L is the cloud liquid water at the ith level. The vertical integral of $[\mathrm{DCP}]_i$ over all the model levels give the surface reaching DCP.

4 Results

4.1 Tropical intraseasonal variability

Figure 1 shows the time-longitude diagrams of precipitation in the equatorial belt (5°S–5°N) for a 90-day period from the control simulation (CTRL) and experiment (EXPT). Daily data for the period starting on the 180th day of the model run to the 269th day have been used for the analysis. In both the simulations, precipitation bands are moving eastward (green lines on the figure show two examples) resembling equatorial moist Kelvin waves (Wheeler and Kiladis 1999). These precipitation bands are propagating with zonal wavenumber 1–2 at intraseasonal time scales; these are the active phases of ISV. However, there are some notable differences between the two simulations. Firstly, the phase speed of the ISV is slower in EXPT than in CTRL. Secondly, the propagation is more prominent, organized, and coherent in EXPT. In CTRL, precipitation appears in non-contiguous patches that indicate lack of convective organization. Thirdly, the active phases of the ISV constitute hierarchical sub structures embedded within them, which are absent in the CTRL case. Within the active phases of the ISV, there are distinct eastward propagating super clusters of spatial scale of several thousand kilometers and time scale of several days. Within the super clusters, there are westward propagating clusters of spatial scale of several hundred kilometers and time scales of few days (blue lines in the figure). The hierarchical structure of ISV is similar to that shown by Nakazawa (1988) from satellite observations. Many models fail to simulate these intricate hierarchical structures of the ISV (Hayashi and Golder 1986; Lau and Waliser 2005). These models simulate the super clusters, but generally fail to capture the clusters that are embedded in them. Nakazawa (1988) stated that the treatment of cumulus parameterization is the key to simulate these intricate features of the tropical convection; indeed changing of τ helps in improving the hierarchical structure of the ISV.

We further analyzed each component of the precipitation, i.e., DCP, SCP, LSP. Figure 2 shows the longitude-time distributions of DCP, SCP, and LSP from the CTRL and EXPT. Close inspection of the figure reveals that change in τ leads to change in the proportion of the precipitation components. In the equatorial belt, the proportion of DCP, SCP, and LSP has changed from (95.3, 3.4, 1.3%) to (31.5, 57.7, 10.8%). DCP was the major component in CTRL, with very little SCP and LSP. But when τ was increased, there is a substantial enhancement in SCP accompanied with a decrease in DCP and a little increase in LSP. It is noticed that SCP has more organizational characteristics than DCP (see a1 and b2). Hence, increase in the proportion of SCP results in an enhancement in the organization of ISV.

4.2 Convectively coupled equatorial waves

A large part of the synoptic variability in the tropics is due to the zonally propagating disturbances. These zonally propagating disturbances move along the equator are often referred as the equatorial waves in the literature. Wavenumber–frequency spectral analysis of outgoing long wave radiation (OLR) was carried out, using the method proposed by Wheeler and Kiladis (1999, hereafter referred to as WK99). As WK99 stated, relying on the assumption that OLR is a reasonably good representation of deep tropical cloudiness, these disturbances are referred as CCEW. The convectively coupled equatorial waves comprise of a spectrum of wave disturbances of varying wavenumber, frequency and power. Some of them, which are discussed in the following are, Kelvin, $n = 1$ equatorial Rossby (ER), mixed Rossby-gravity (MRG), $n = 0$ eastward inertio-gravity (EIG), $n = 1$ westward inertio-gravity (WIG) waves, and Madden–Julian oscillation (MJO). Figures 3 and 4 show symmetric and antisymmetric components of the normalized power spectra of the OLR averaged from 15°S to 15°N for CTRL, EXPT, and (EXPT–CTRL). This normalization procedure removes a large portion of the systematic biases within the models, and more clearly displays the model disturbances with

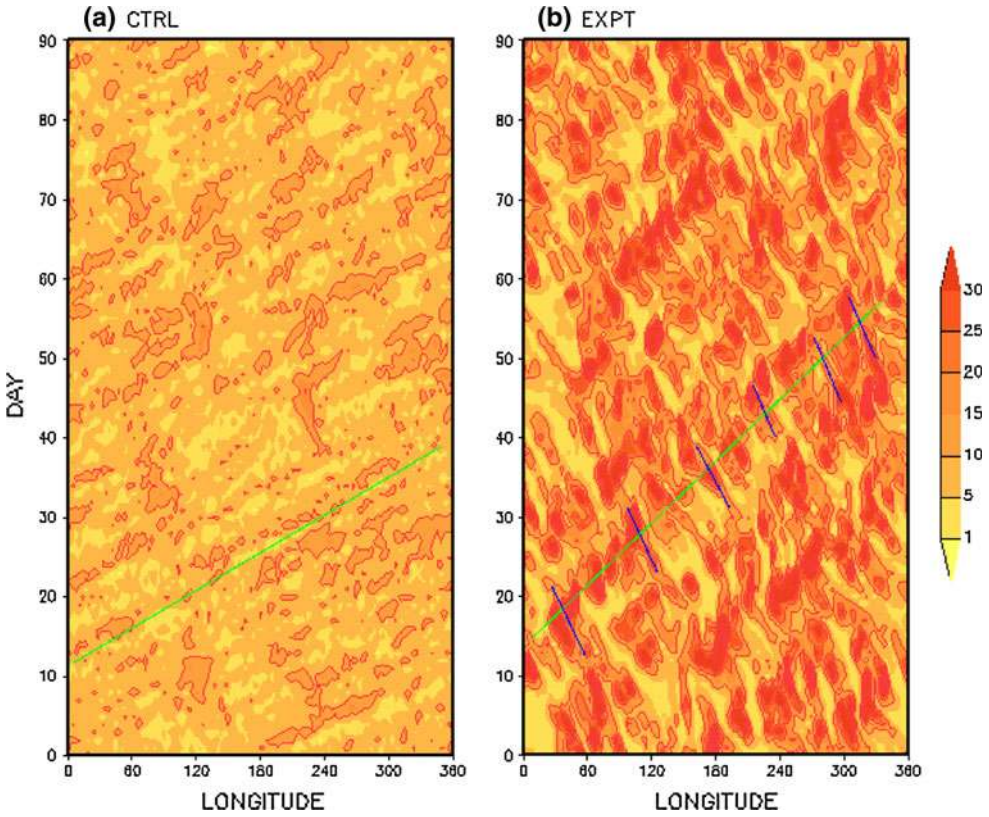

Fig. 1 Longitude–time diagrams of precipitation rates (mm/day) averaged between 5°S and 5°N obtained from **a** CTRL, and **b** EXPT

respect to their own climatological variances at each scale. The conventional dispersion curves of shallow water modes for equivalent depths of 12, 25, and 50 m are shown in the figures.

Figure 3 reveals that, in CTRL, the Kelvin waves have most of their variance centered on an equivalent depth of approximately 50 m corresponding to a speed of 22.1 m/s. The variance in EXPT centers around a 25-m equivalent depth, which is corresponding to 15.6 m/s. This indicates a reduction in the phase speed of Kelvin waves with increases in τ. In addition to that there is a reduction in power in the low-frequency regime (below 5 days period) of Kelvin waves. The MJO is another eastward propagating mode with period 30–70 days and wavenumbers 1–5. Both the simulations show some variance within these bands, MJO is more energetic in EXPT. In Fig. 3, the westward propagating waves at wavenumber 1–10 and period 10–45 days are the ER waves. Both the simulations have problem in simulating the ER waves, especially at higher scales. But, comparatively EXPT performs a better simulation. WIG is another westward propagating wave with wavenumber 1–12 and period below 2.5. These waves are almost absent in the EXPT. The increase in power in ER regime accompanied with a decrease in the WIG regime with increase in τ suggests that the westward propagation becomes more organized and slower, which is also evident in Figs. 1 and 2.

In Fig. 4, the eastward propagating antisymmetric waves at wavenumber 1–12 and period 2–4 days are the EIG waves. The figure shows that there is a substantial increase in power in this regime with increase in τ. The westward propagating waves in Fig. 4 at wavenumber 1–10 and period 3–7 days are the MRG waves. Increase of τ leads to an increase in power in the larger scales regime, however, in the smaller scales the reverse has happened. The bull's eye around wavenumber 4–8 and 10–20 days in CTRL is an artifact, which has been resolved in EXPT.

4.2.1 Relative importance of precipitation components

It is seen that changing of τ leads to the change in the proportion of the precipitation components, i.e., DCP, SCP, and LSP. Since these three components are different in their characteristics, importance of each component in the simulation of convectively coupled equatorial waves is desirable. To examine this, a set of six simulations was carried out. In three simulations, only one precipitation scheme was allowed to operate at a time. For example, "SCP & LSP switched off" is a case (refer to Fig. 5) in which only DCP is operating. Similarly, in the remaining three simulations one scheme was switched off at a time. For instance, "LSP switched off" is the case in which LSP is switched off but both DCP and SCP are operating. The

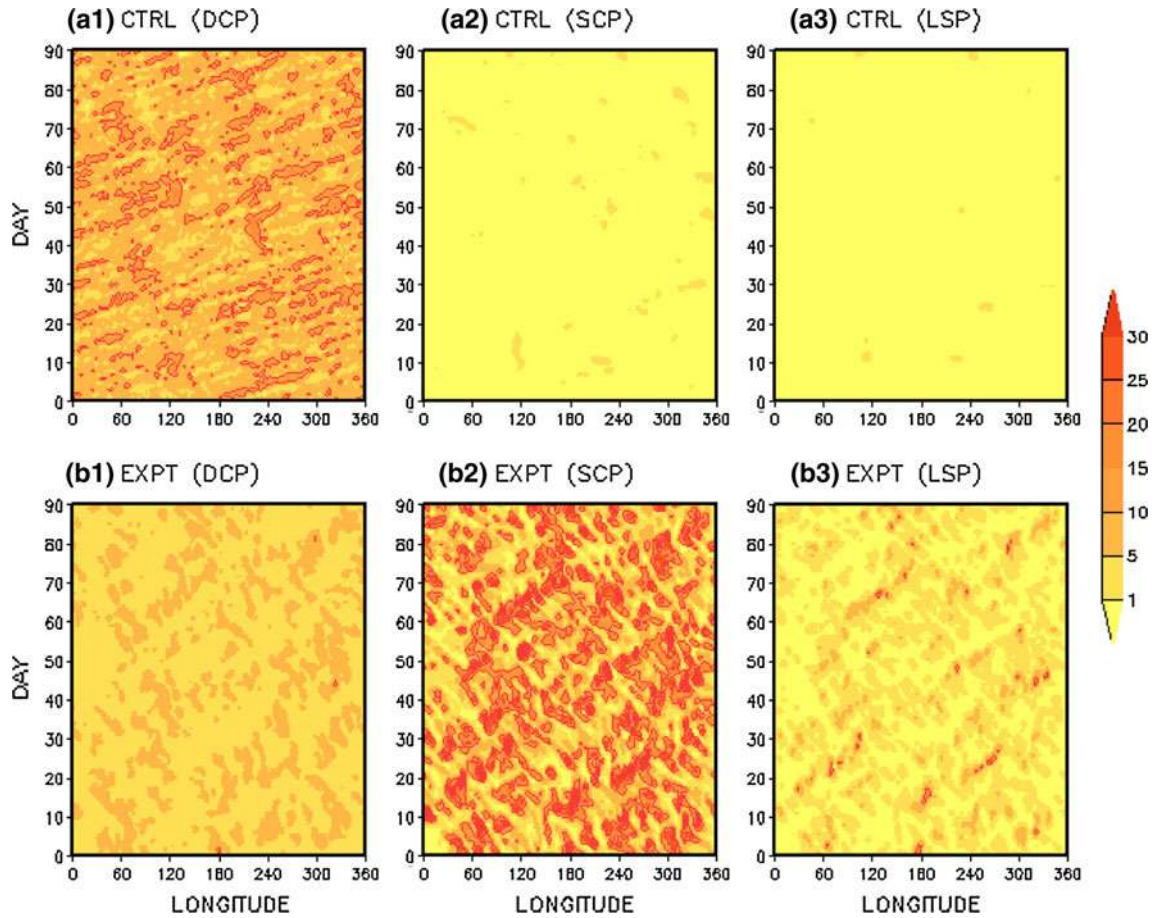

Fig. 2 As in Fig. 1, but for deep convective precipitation (DCP), shallow convective precipitation (SCP), and large- scale precipitation (LSP)

results of these simulations are shown in Fig. 5 (symmetric components) and in Fig. 6 (antisymmetric components).

From the top panel of Fig. 5, it is noticed that neither DCP scheme (Fig. 5a) nor SCP scheme (Fig. 5b) could simulate the symmetric components of convectively coupled equatorial waves when operating alone. Whereas, when LSP scheme is operating alone (Fig. 5c), considerable power is found in the wavenumber–frequency spectra, and some of the power peaks follow the dispersion curves of the equatorially trapped waves. On the other hand, Fig. 5d shows that when the LSP scheme is switched off, the power in the wavenumber–frequency domain is reduced significantly. Moreover, Fig. 5c shows that the simulated Kelvin waves follow the dispersion curve of relatively lower equivalent depths, and MJO possess reasonable power at lower wavenumbers. When the SCP scheme is switched off but DCP and LSP schemes operate, there is considerable power, but the eastward propagation is too fast, and unrealistic power at higher frequencies are noticed. Figure 5f shows that when DCP is switched off, Kelvin waves follow the 25 m equivalent depth dispersion curve. However, switching off the DCP leads to significant reduction of power in the MJO regime. Hence, it is inferred that lower fraction of SCP and LSP leads to too fast eastward propagation, excess power at higher frequency Kelvin waves, and weaker MJO. Similarly, the figure reveals that LSP is important for the simulation of ER, and when it operates ER becomes energetic otherwise not.

Similarly, Fig. 6 shows the role of each precipitation component on the simulation of the antisymmetric component of the convectively coupled equatorial waves. It is noticed that when LSP is switched off (Figs. 6a, b, d), spurious power appears at all the wavenumbers and frequencies with some unreasonable pronounced spectral peaks between wavenumbers 2 and 10 and periods 3 and 30 days. However, in the reverse scenario, e.g., when LSP operates but SCP or/and DCP are switched off, these spurious power and unrealistic spectral peaks in the above-mentioned regime disappeared. This indicates that LSP has key role in simulating the antisymmetric components of the CCEW. Moreover, when LSP and DCP schemes operate but SCP is switched off (Fig. 6f), both MRG and EIG waves become energetic. On the contrary, when LSP and SCP operate EIG waves are energetic but MRG waves become weak. This implies that increase in the proportion of SCP leads to a decrease in the power of the MRG waves.

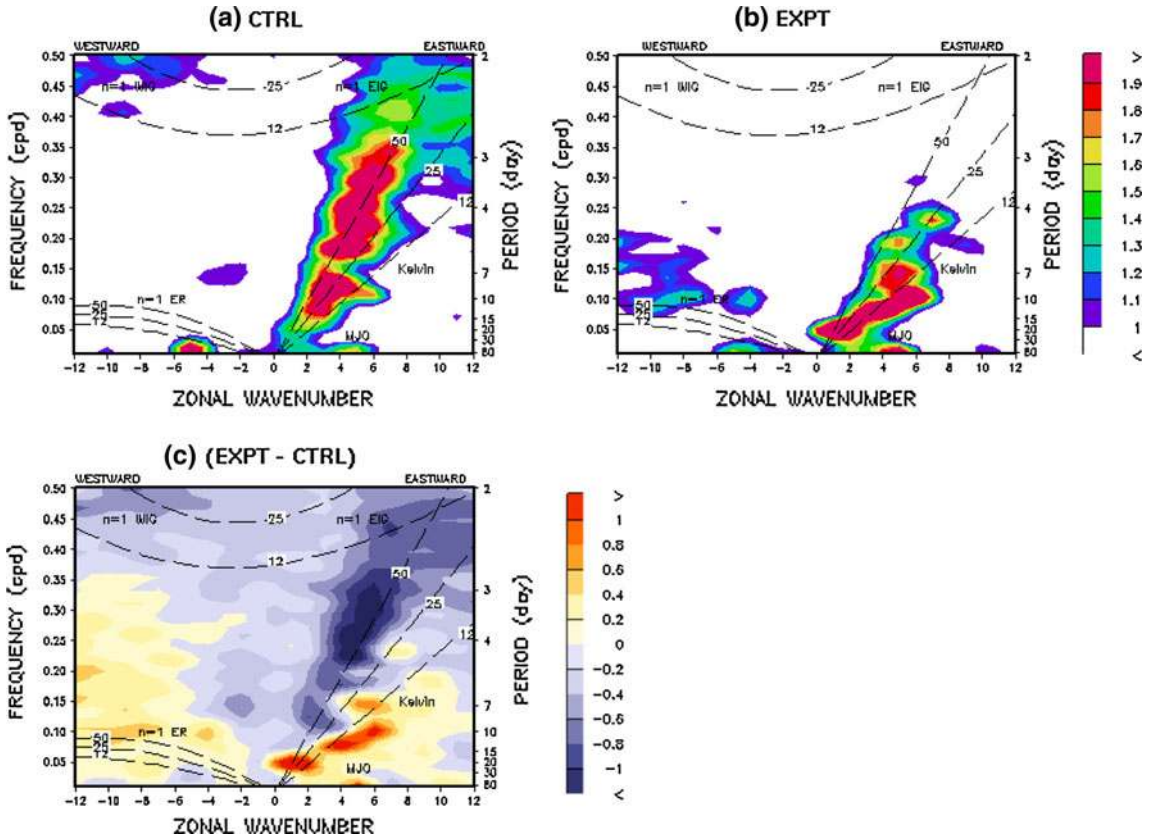

Fig. 3 The symmetric component of the wavenumber–frequency distribution of OLR averaged between 15°S and 15°N is shown for **a** CTRL, **b** EXPT, and **c** (EXPT–CTRL)

When τ was increased, the proportion of SCP was increased significantly accompanied with a marginal increase in LSP that caused the slowing down of Kelvin waves, more energetic MJO, ER, EIG waves and weakening of the MRG waves.

4.2.2 *Evaporation convection coupling*

Figure 7 shows the longitude–latitude composite diagrams of anomalous precipitation rates (mm/day) and surface evaporation (mm/day) from the EXPT. In Fig. 7a, it is noticed that there is an anomalous convective center over equator, extending from 60° to 120°. In the bottom panel (see Fig. 7b), it is seen that there is an anomalous evaporation occurring over 70°–240°. This anomalous evaporation covers several thousand kilometers along the east of the convective center, whereas, to the west of the convective center the evaporation is noticed to be suppressed. In CTRL, The zonal asymmetry in surface evaporation is not as prominent (not shown here). So it is thought that the effects of τ seen in the preceding sections might be due to a stronger coupling between surface evaporation and convection. To investigate this issue, simulations were carried out, in which same zonally symmetric evaporation was prescribed to both the simulations. The prescribed evaporation was constructed from 12 months mean evaporation of CTRL run, by averaging in the zonal direction. Figure 8 shows the symmetric component of the convectively coupled equatorial waves with prescribed evaporation. It is noticed that Kelvin waves and MJO become weak with increase in τ when the zonal asymmetry in surface evaporation was seized. This implies that increase in τ leads to a better coupling between surface evaporation and convection, which develops zonally asymmetry in surface evaporation across the convective center and gives more energetic eastward propagation. However, the increase in power of ER with increase in τ is not due to a stronger coupling between convection and surface evaporation, since the effects of TAU on this regime is similar even when the coupling is seized. The antisymmetric components are also found to be insensitive to the coupling (not shown here).

4.2.3 *Moist heating*

Diabatic heating is central to the structure and propagation of the eastward propagation (Krishnamurti et al. 1985; Murakami and Nakazawa 1985; Yanai et al. 2000). There

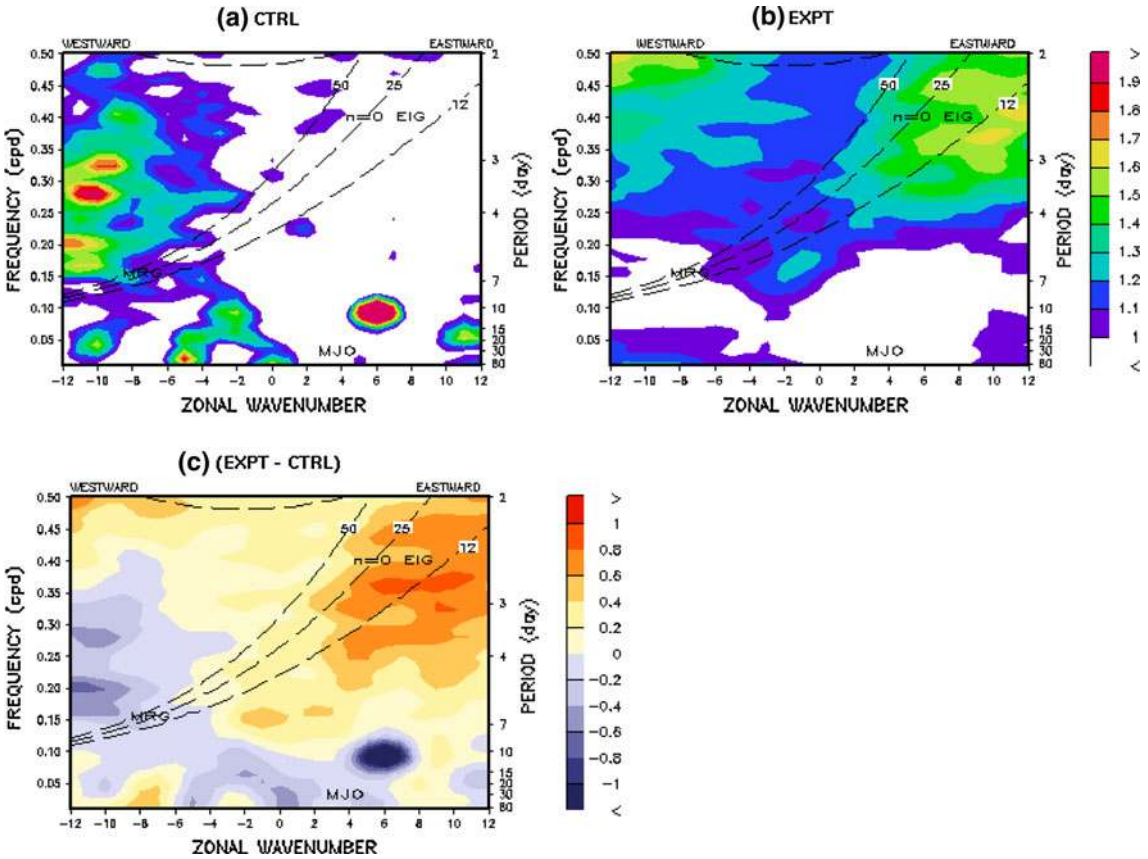

Fig. 4 The antisymmetric component of the wavenumber–frequency distribution of OLR, averaged between 15°S and 15°N is shown for **a** CTRL, **b** EXPT, and **c** (EXPT–CTRL)

are several wave-CISK studies, which addressed the dependence of phase speed of Kelvin waves on the altitude of maximum heating. Takahashi (1987) and Lau et al. (1988) used linearized heating and showed that phase speed decreases with decrease in the altitude of the maximum heating. Using conditional ("positive only") heating, Lau and Peng (1987) and Sui and Lau (1989) showed similar dependence of phase speed. A consistent result was shown from a full GCM study by Tokioka et al. (1988). Park et al. (1990) examined ISVs in three different GCMs and concluded the same. Lin et al. (2004), based on the dynamics of adiabatic Kelvin wave, explained that bottom heavy heating profile tends to excite waves with short vertical wavelength, which propagates slowly. Diabatic heating mainly constitutes of latent heating due to the moist processes and radiative heating due to clouds and radiatively active atmospheric constituents. We noticed that radiative heating profile does not change significantly with τ. However, the profile of moist heating is influenced by τ (see Fig. 9). Increase of τ leads to lowering of the altitude of maximum heating. Therefore, based on the perspective of the above-mentioned previous studies, lowering of the altitude of the maximum heating would reduce the phase speed of Kelvin waves. When τ increases, rate of DCP decreases accompanied with an increase in SCP and LSP, predominantly the SCP. This alters the profile of the precipitation production from a vertically extended profile to a bottom heavy one due to more contribution from shallow convection and in turn lowers the altitude of maximum.

4.3 Diurnal and sub-diurnal variability

Figure 10 shows the power spectrum of precipitation for CTRL and EXPT. The spectra are based on 90 days time series, with period greater than 24 h filtered out. In CTRL, most of the power lies in the off-equatorial region, whereas in EXPT, it lies in the equatorial region. This is consistent with the location of the time-mean precipitation peaks shown in Mishra and Srinivasan (2010). In both the simulations, the power at the diurnal scale (24-h period) is prominent. It is noticed that in most of the frequencies, the power in EXPT is lower than that in CTRL, over most of the latitudes. This result contains the clue that higher τ could reduce the frequency of precipitation at sub-diurnal scales.

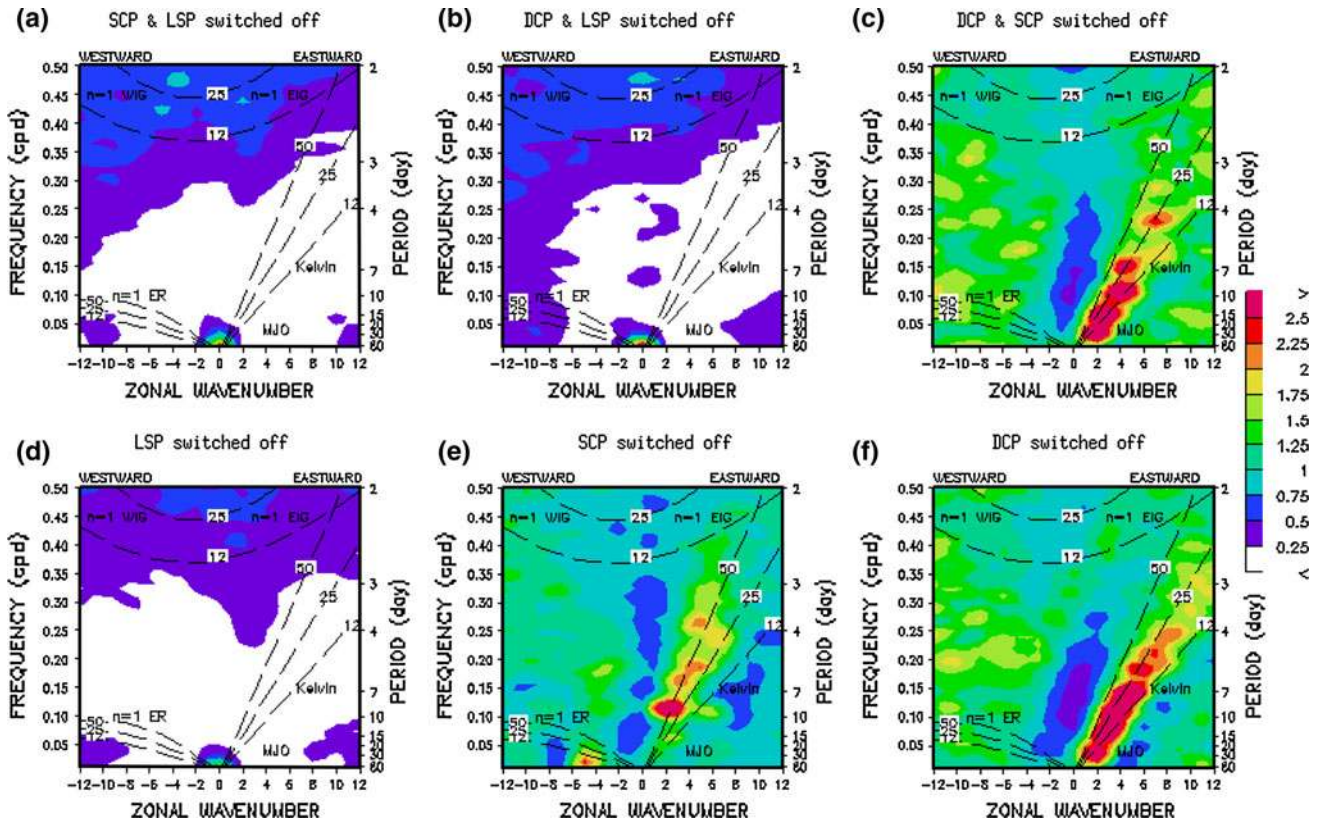

Fig. 5 The symmetric component of the wavenumber–frequency distribution of OLR averaged between 15°S and 15°N is shown for **a** SCP & LSP switched off, **b** DCP & LSP switched off, **c** DCP & SCP switched off, **d** only LSP switched off, **e** only SCP switched off, and **f** only DCP switched off

Figure 11 shows composite diurnal cycles for four regions on and off the equator for CTRL and EXPT. These composites are constructed from hourly data of 90 days time series from each simulation. Latitudinal locations of the boxes were selected in raining latitudes; however, the longitudinal locations were arbitrarily chosen. It is noticed from the figure that diurnal cycle of both the simulations are in phase, in all the boxes. However, the amplitude of diurnal variation is affected by τ. In the off-equatorial boxes (see plots b1 and b3), the amplitude is lower with EXPT. However, in the equatorial boxes (see plot b2 and b4) the amplitude in both the simulations is found to be largely equal, although the mean diurnal precipitation in EXPT is larger than that in CTRL in these boxes.

Figure 12 shows time series of precipitation simulated by CTRL and EXPT in the same four boxes. It is noticed that CTRL is raining continuously; on the contrary, EXPT is raining intermittently with distinct active and break phases. In addition, the range of variation of precipitation is higher in EXPT. Similarly, Fig. 13 shows for CAPE from both the simulations. In CTRL the CAPE varies in a range of 0–500 J/kg, which is too low as compared to the tropical atmosphere. But in EXPT, it varies more reasonably in a range of 0–2,000 J/kg with remarkable high and low phases. Some other time series were also examined and similar results were obtained.

4.4 Intensity and frequency of precipitation

To examine the impact of τ on the intensity and frequency of precipitation, the daily precipitation rates for a 90-day period was analyzed. Figure 14 shows the frequency distribution (left panel) and the total precipitation falling in each bin (right panel), in the deep tropics, i.e., 0°–360° and 12.5°S–12.5°N. Based on the intensity, the precipitation rates are categorized into five categories, namely, dry, light, moderate, heavy, and very heavy. In EXPT, the frequencies in the dry, heavy, and very heavy categories have been found to increase, whereas in the light and moderate categories it has decreased. The accumulated precipitation is found to increase in dry, heavy and very heavy categories, while it decreases in the light and moderate categories. This indicates that increase of τ leads to a more extreme situation, i.e., when it rains it pours. We showed that increasing of τ leads to higher CAPE in the atmosphere. Because of that when there is large-scale

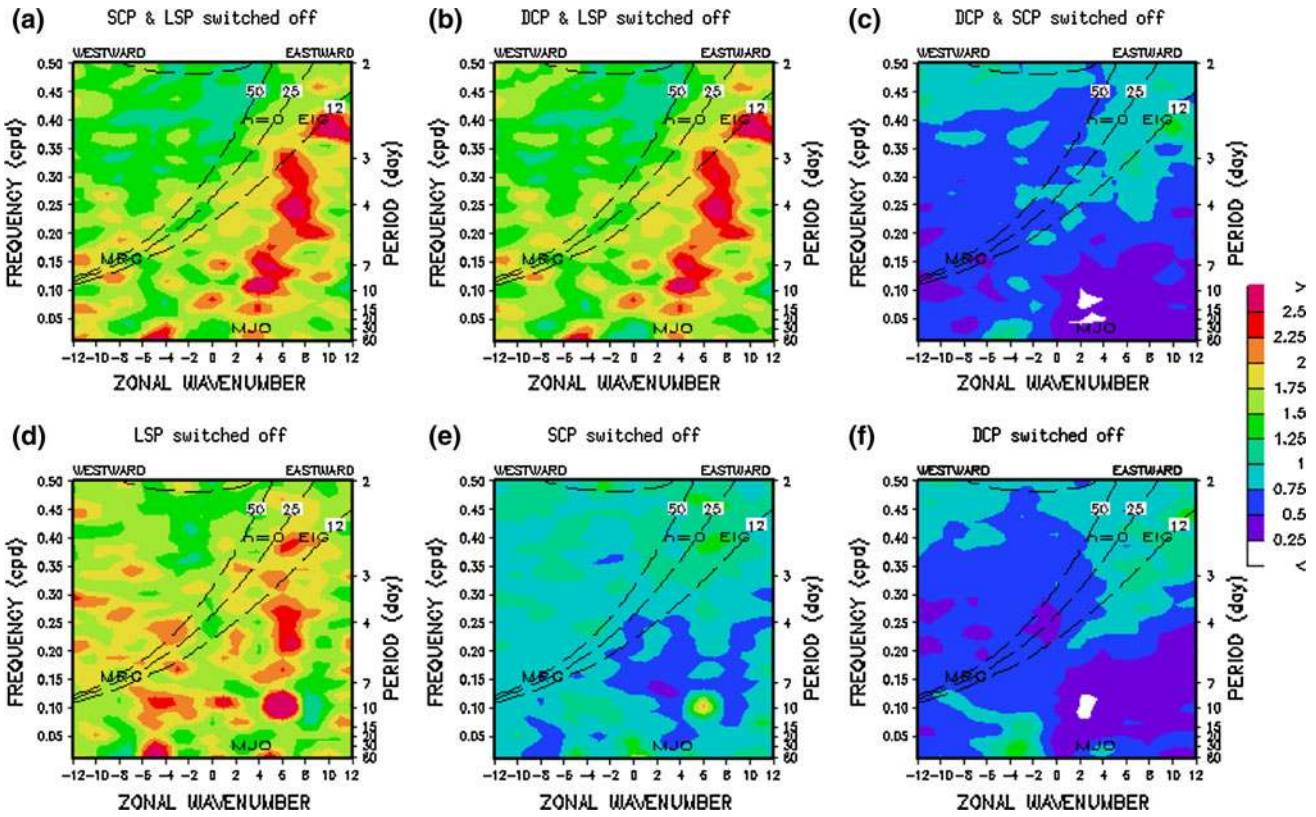

Fig. 6 The antisymmetric component of the wavenumber–frequency distribution of OLR, averaged between 15°S and 15°N is shown for **a** SCP & LSP switched off, **b** DCP & LSP switched off, **c** DCP & SCP switched off, **d** only LSP switched off, **e** only SCP switched off, and **f** only DCP switched off

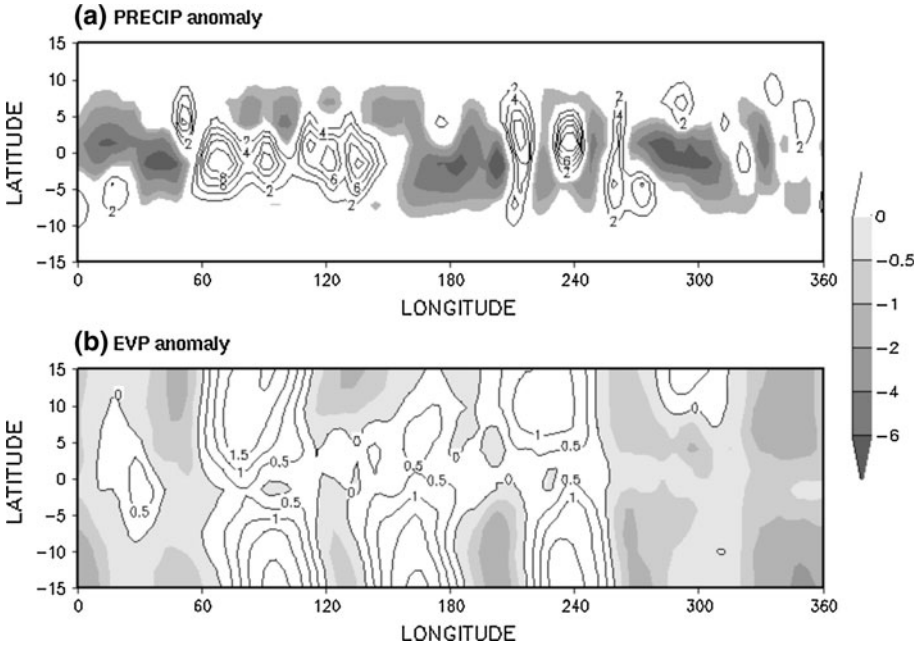

Fig. 7 Longitude–latitude composite diagrams of **a** precipitation rates (mm/day) for EXPT, and **b** surface evaporation (mm/day) for EXPT. Zonal means are removed and negative values are *shaded* and positive values are *contoured* in each plots

convergence, the atmosphere has the potential to release the CAPE, which is a favorable condition for the extreme events to occur.

Figure 15 shows a similar plot, but here, DCP, SCP, and LSP are shown individually. It is seen that increase of τ leads to a decrease in the frequency of DCP in the

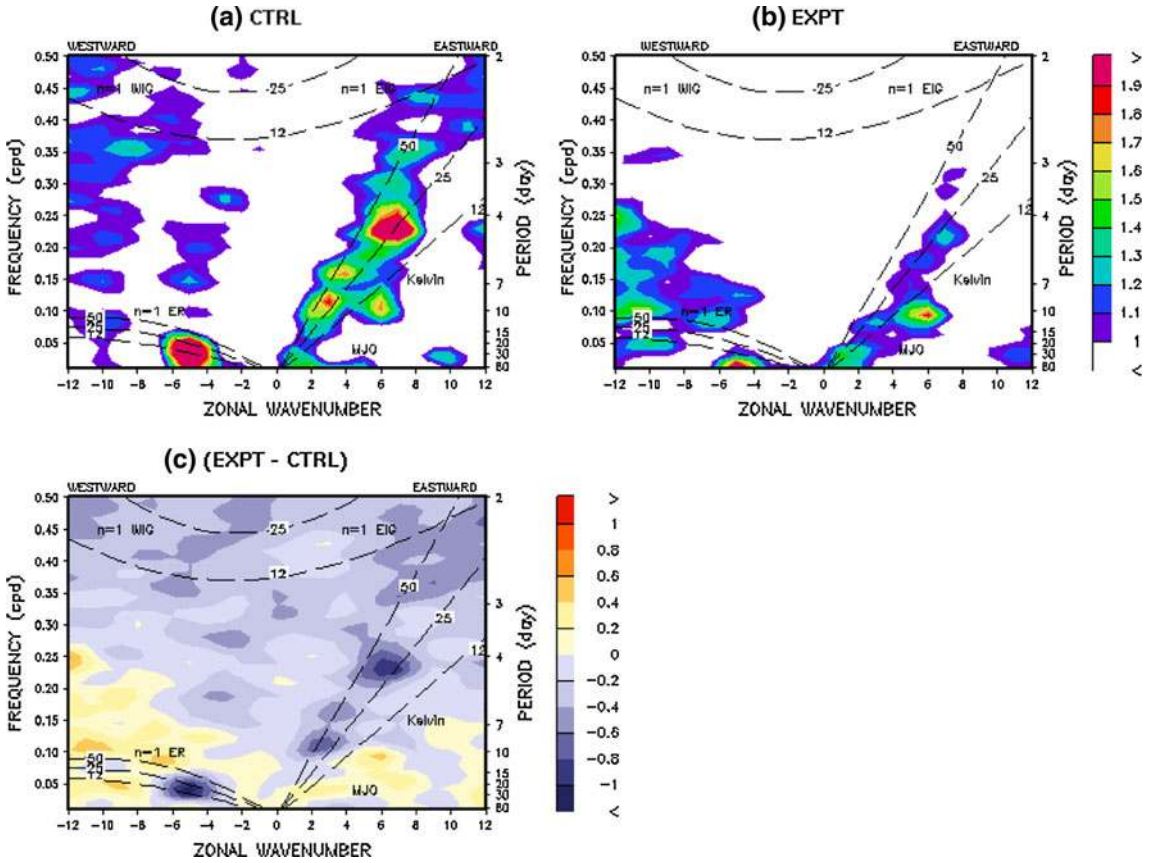

Fig. 8 The symmetric component of the wavenumber–frequency distribution of OLR, averaged between 15°S and 15°N, from the zonally symmetric evaporation experiment are shown for **a** CTRL, **b** EXPT, and **c** (EXPT–CTRL)

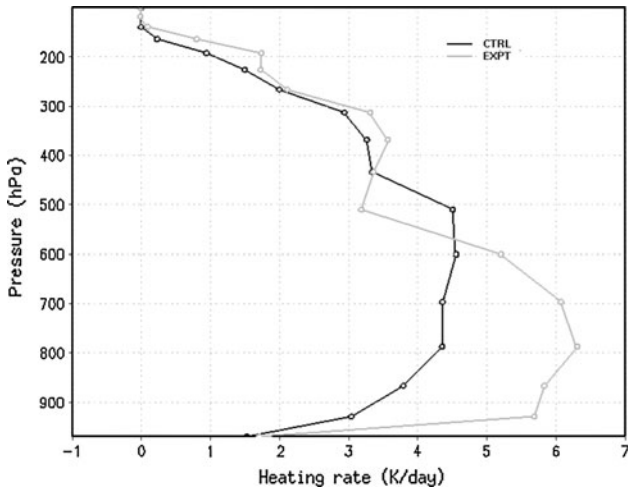

Fig. 9 Vertical structure of the area averaged (0–360°E and 7°S–7°N) heating rate due to the moist processes form CTRL and EXPT

higher intensity categories and increase in the lower intensity categories. On the other hand, SCP and LSP respond just in the opposite way, i.e., frequencies increase in the higher intensity categories and decrease in the lower intensity categories. Shallow convection contributes more to high precipitation events than deep convection.

4.5 Real-planet simulations

To see how the effects of τ in aqua-planet translate to the real-planet, simulations were performed with full AGCM. Two 10-year (Jan. 1979–Dec. 1988) long simulations were performed with observed SSTs, i.e., one with $\tau = 1$ h (CTRL), and another with $\tau = 8$ h (EXPT). We analyzed the daily model outputs, and examined some of the transient activities from both the simulations.

Figures 16 and 17 show the symmetric and antisymmetric components of the convectively coupled equatorial waves, respectively. It is noticed that increase of τ leads to decrease in the phase speed of Kelvin waves from 50 to 25 m equivalent depth. The variance over the MJO and ER increases. EIG becomes marginally stronger and MRG becomes weaker. These effects are in the same line as those seen in the aqua-planet framework.

We further analyzed the daily data to examine the response of intensity and frequency of precipitation in the

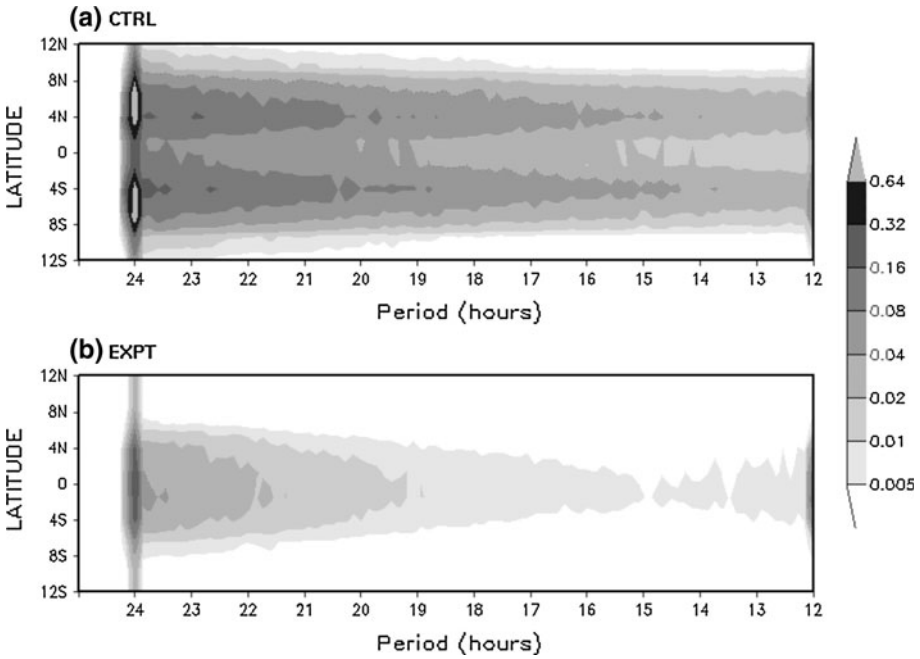

Fig. 10 The power spectrum of hourly precipitation from **a** CTRL, and **b**2 EXPT case is plotted as a function of latitude and period. The spectra are based on 90 days time series, with periods greater than 24 h filtered out. Unit is mm^2/day

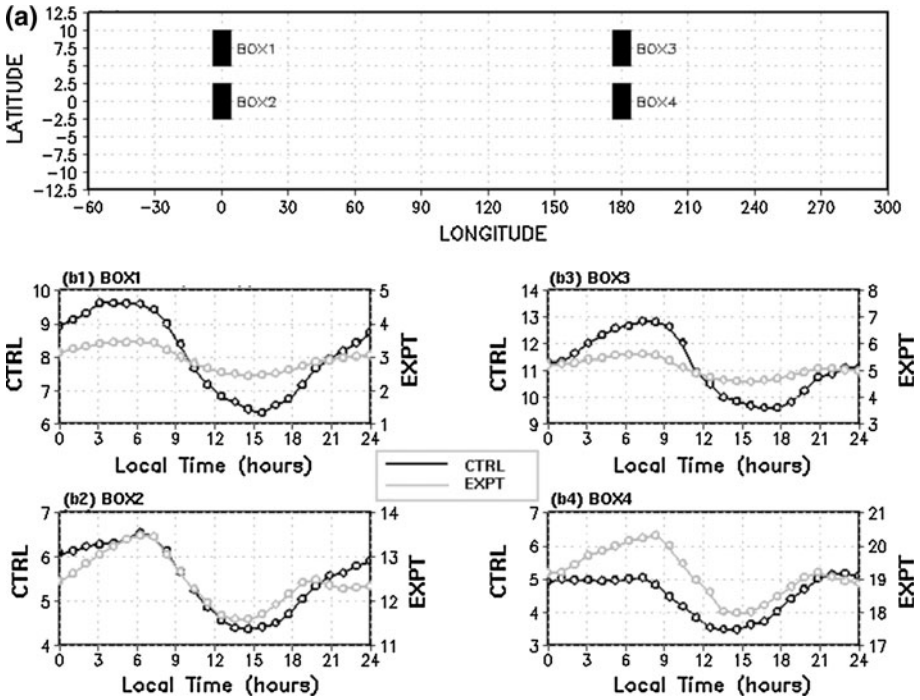

Fig. 11 Diurnal cycle of precipitation constructed from the hourly output of 90 days data for CTRL and EXPT, for the four boxes shown in **a**. **b1** Shows the diurnal cycle for *box1*, **b2** shows the diurnal cycle for *box2*, **b3** shows the diurnal cycle for *box3*, and **b4** shows the diurnal cycle for *box4*

tropics. The frequency distribution and the total precipitation falling in each bin are shown in Fig. 18. The frequencies in the dry, heavy, and very heavy categories have been found to increase with EXPT (see Fig. 18a), whereas in the light and moderate categories the reverse has been noticed. Similarly, Fig. 18b shows that the accumulated precipitation increases in dry, heavy and very heavy categories, and decreases in the light and moderate categories. Therefore, higher τ leads to an extreme situation, i.e., it does not rain always but when it rains it pours. Similarly, DCP, SCP, and LSP are shown individually in Fig. 19. It is noticed that increase of τ leads to a decrease in the frequency of DCP in the higher intensity categories and increase in the lower intensity categories, whereas in the case of SCP and LSP it does the opposite. The over all characteristics of the tropical transient activities and their response to τ is found to be similar in both the planets.

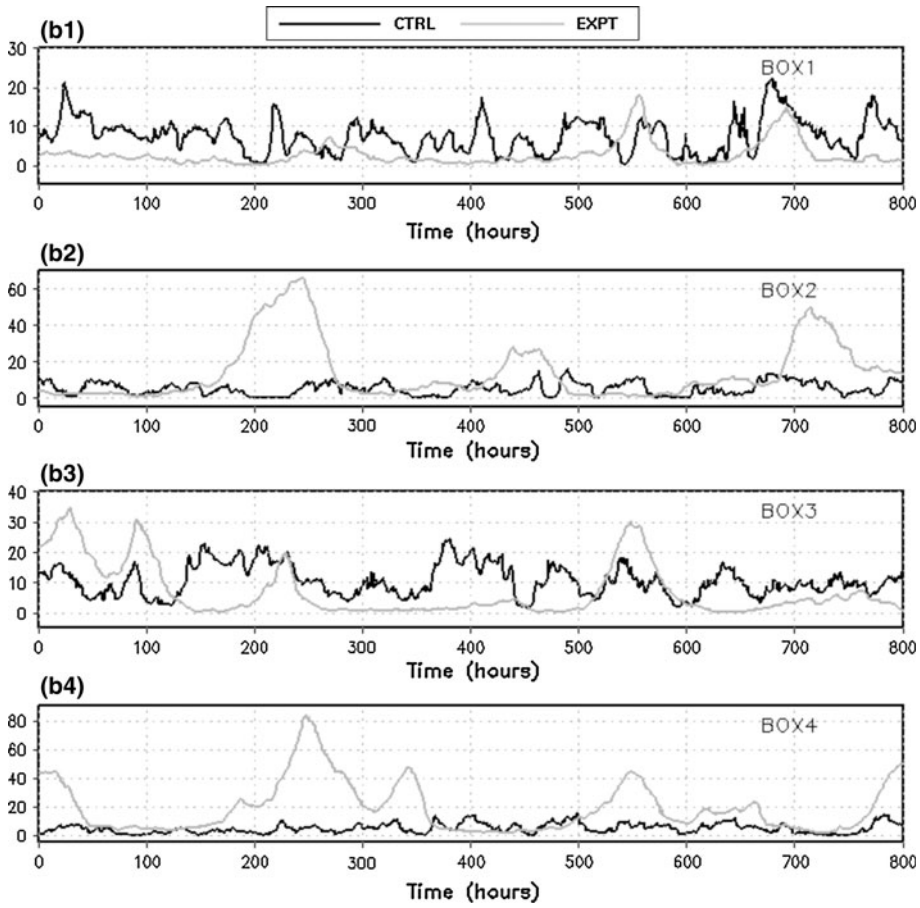

Fig. 12 Variation of precipitation over the four boxes of Fig. 11. Hourly data has been used

5 Summary and discussions

The influence of convective adjustment time scale (τ) on the tropical transient activity is investigated using NCAR-Community Atmosphere Model version 3 (CAM3). τ is a characteristic time scale with which CAPE is removed at an exponential rate by convection. In the default configuration of the model, the value of τ is 1 h. Some recent observational findings suggest that it is larger by around one order of magnitude. Subsequently modeling study demonstrated its impact on mean climate. To see if alteration of this time scale could affect transient features of climate, numerical experiments are performed using aqua-planet and real-planet frameworks. Since aqua-planet is a simpler setting with fewer feedbacks, it is easier to understand the effect and underlying processes. Finally the real-planet framework with actual land, ocean, and sea ice distribution is used to see if the facts understood in the aqua-planet configuration works similarly in the real-planet configuration or not. Various aspects of the transient climate, i.e., ISV, CCEW, diurnal and sub-diurnal variability, and intensity and frequency of precipitation, are analyzed in this study.

As mentioned in the preceding discussion, recent observational studies suggest using a longer τ, and recent modeling studies suggest to use 8 h. In order to see if using 8 h could make any difference, two simulations are performed in the aqua-planet framework, one with a time scale of 1 h (CTRL) and another with 8 h (EXPT). Remarkable differences are noticed in the transient features. In EXPT, ISV is more reasonable that constitutes hierarchical sub structures embedded within them during the active phases. Within the ISV, there are distinct eastward propagating super clusters of spatial scale of several thousand kilometers and time scale of several days. Within the super clusters, there are westward propagating clusters of spatial scale of several hundred kilometers and time scales of few days. The hierarchical structure of ISV is absent in CTRL. In CTRL, the Kelvin waves have most of their variance centered on an equivalent depth of approximately 50 m corresponding to a speed of 22.1 m/s. The variance in EXPT centers on a 25 m equivalent depth, which is corresponding to 15.6 m/s. This indicates a reduction in the phase speed of Kelvin waves with increases in τ. The MJO is more energetic and, $n = 1$ ER and $n = 0$ EIG waves are more prominent in EXPT. There is an increase in power in

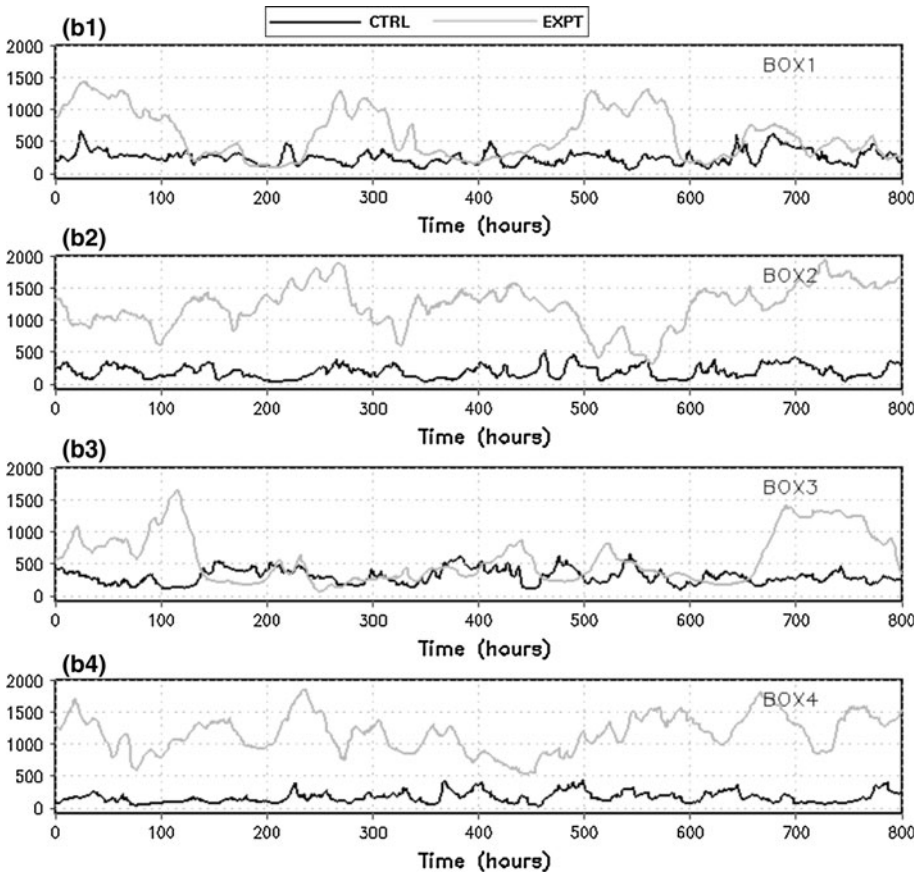

Fig. 13 Variation of CAPE over the four boxes of Fig. 11. Hourly data has been used

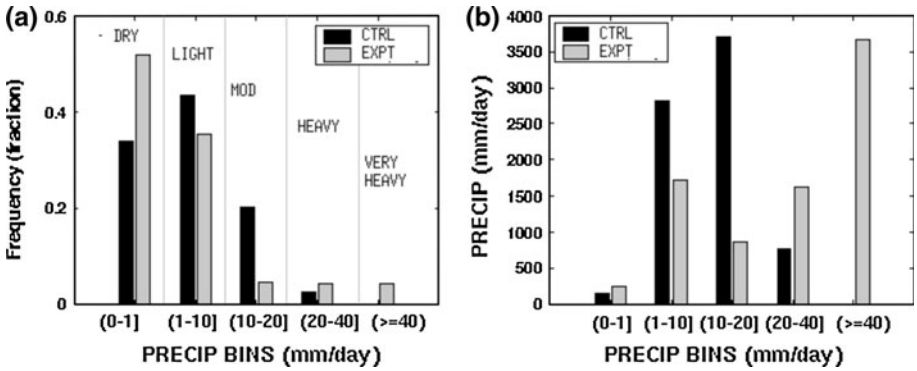

Fig. 14 **a** Frequency distribution of daily precipitation rates in the deep tropics (0–360°E and 12.5°S–12.5°N) for 90 days. **b** Amount of precipitation falling in each bin of precipitation rates

the larger scales regime of the MRG waves. However, the power in the smaller scales regime of MRG waves and in the WIG modes goes down. In CTRL, a bull's eye appear around wavenumber 4–8 and 10–20 days, which has been resolved in EXPT.

It is seen that changing of τ leads to change in the proportion of the precipitation components, i.e., DCP, SCP, and LSP. Since the three components are different in their characteristics, importance of each component in the simulation of convectively coupled equatorial waves are different. An additional set simulation was carried out isolating the effect each component on CCEWs and concluded that the slowing down of Kelvin waves and increase in the power in the MJO modes is primarily due to the increase in the proportion of SCP; and increase in the power in the ER mode is due to increase in the proportion of LSP.

Longitude–latitude composite diagrams of anomalous precipitation and surface evaporation are analyzed from CTRL and EXPT. In EXPT, anomalous surface evaporation occurs over several thousand kilometers along the east of the convective center, whereas, to the west of the convective center the evaporation is suppressed. In CTRL, the zonal asymmetry in surface evaporation is not that

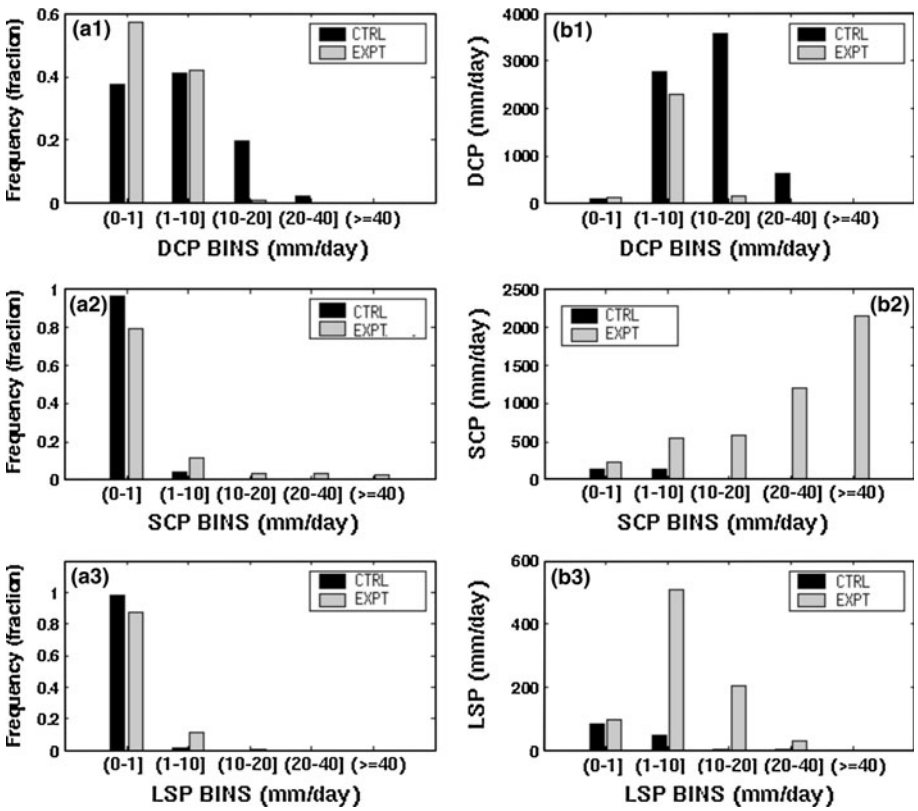

Fig. 15 **a1** Frequency distribution of daily deep convective precipitation rates in the deep tropics (0–360°E and 12.5°S–12.5°N) for 90 days, **b1** amount of deep convective precipitation falling in each bin of precipitation rates, **a2** as in **a1**, but for shallow convective precipitation, **b2** as in **b1**, but for shallow convective precipitation, **a3** as in **a1** but for large-scale precipitation, and **b3** as in **b1** but for large-scale precipitation

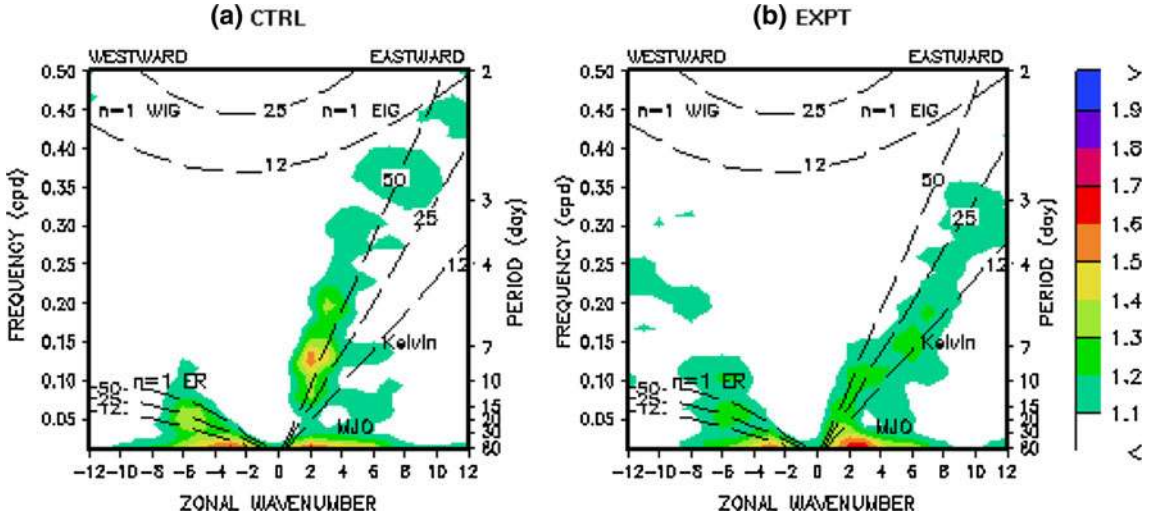

Fig. 16 The symmetric component of the wavenumber–frequency distribution of OLR averaged between 15°S and 15°N is shown for **a** CTRL, and **b** EXPT

prominent. So it is apparent that the effects of τ might be due to a stronger coupling between surface evaporation and convection. To investigate this issue, numerical simulations were carried out, in which same zonally symmetric evaporation was prescribed to both the simulations. The results confirm that increase in τ leads to a better coupling between surface evaporation and convection, which develops zonally asymmetry in surface evaporation across the convective center and gives more energetic eastward propagation. However, ER waves and the antisymmetric components are insensitive to the evaporation–convection coupling.

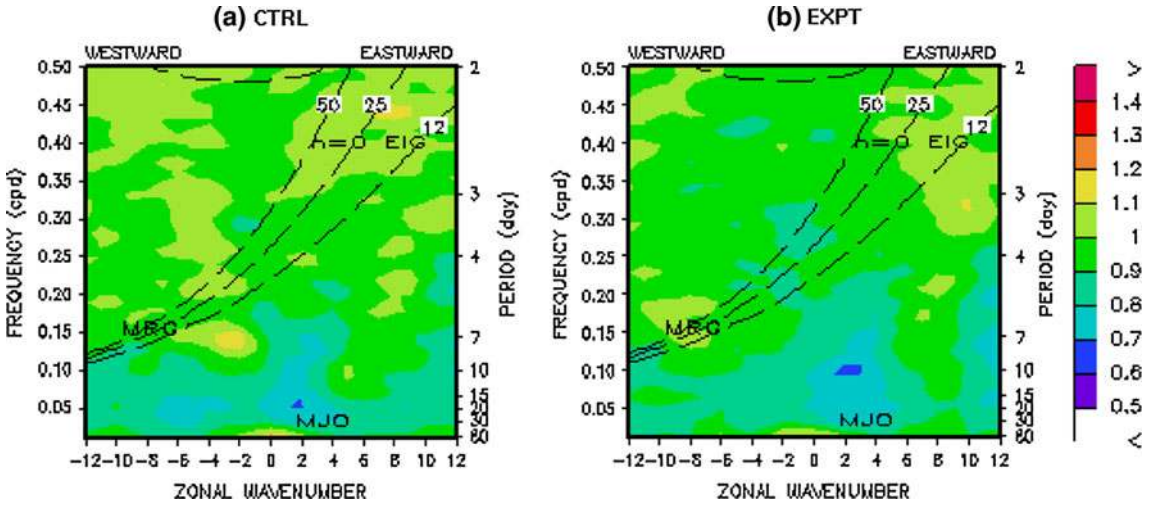

Fig. 17 The antisymmetric component of the wavenumber–frequency distribution of OLR averaged between 15°S and 15°N is shown for **a** CTRL, and **b** EXPT

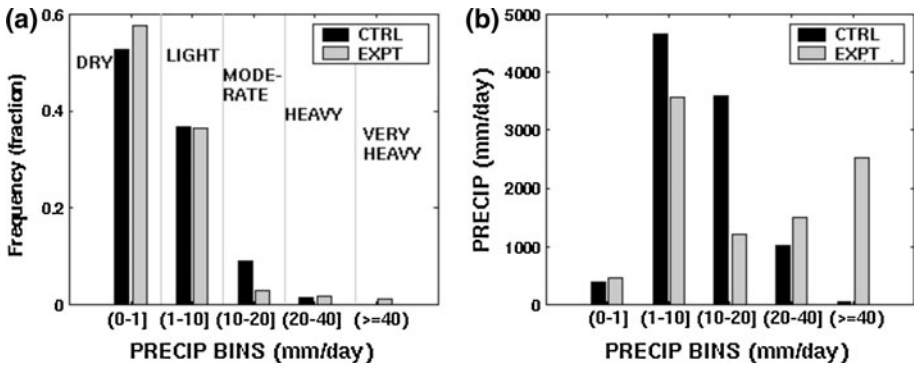

Fig. 18 **a** Frequency distribution of daily precipitation rates in the tropics (0–360°E and 30°S–30°N) for 365 days. **b** Amount of precipitation falling in each bin of precipitation rates

Diabatic heating from CTRL and EXPT is examined, which mainly constitutes of latent heating due to the moist processes and radiative heating due to clouds and radiatively active atmospheric constituents. It is noticed that radiative heating profile does not change so significantly with τ. However, the profile of moist heating is influenced by τ. When τ increases, rate of DCP decreases accompanied with an increase in SCP and LSP, predominantly the SCP. This alters the profile of the precipitation production from a vertically extended profile to a bottom heavy one due to more contribution from shallow convection and in turn lowers the altitude of maximum heating and in turn reduces the phase speed of Kelvin waves.

The amplitude of diurnal variation of precipitation is sensitive to τ. In the off-equatorial regions, the amplitude is lower in EXPT. Over equatorial belt, the amplitude in both the simulations is largely same, though mean diurnal precipitation in EXPT is larger than CTRL. On the contrary, the phase of the diurnal cycle is found to be insensitive to τ. At sub-diurnal scales, the amplitude of variations of precipitation in EXPT is greater. In CTRL, precipitation occurs continuously over the equatorial region. Whereas, it occurs intermittently with distinct active and break phases in EXPT. In addition, the range of variation of precipitation is higher in EXPT. Similarly the CAPE from both the simulations is analyzed. In CTRL, CAPE varies in a range of 0–500 J/kg, which is too low as compared to the tropical atmosphere. But in EXPT, it varies more reasonably in a range of 0–2,000 J/kg with remarkable high and low phases. The intensity and frequency of precipitation are examined from both the cases. Based on the intensity, the precipitation rates are categorized into five categories, viz., dry, light, moderate, heavy, and very heavy. The frequencies in the dry, heavy, and very heavy categories are higher in EXPT, whereas in the light and moderate categories the reverse is true. This indicates that increase of τ leads to a more extreme situation. Additional numerical experimentation in real-planet framework shows similar effects of τ. The overall performance of the model is better when τ is 8 h.

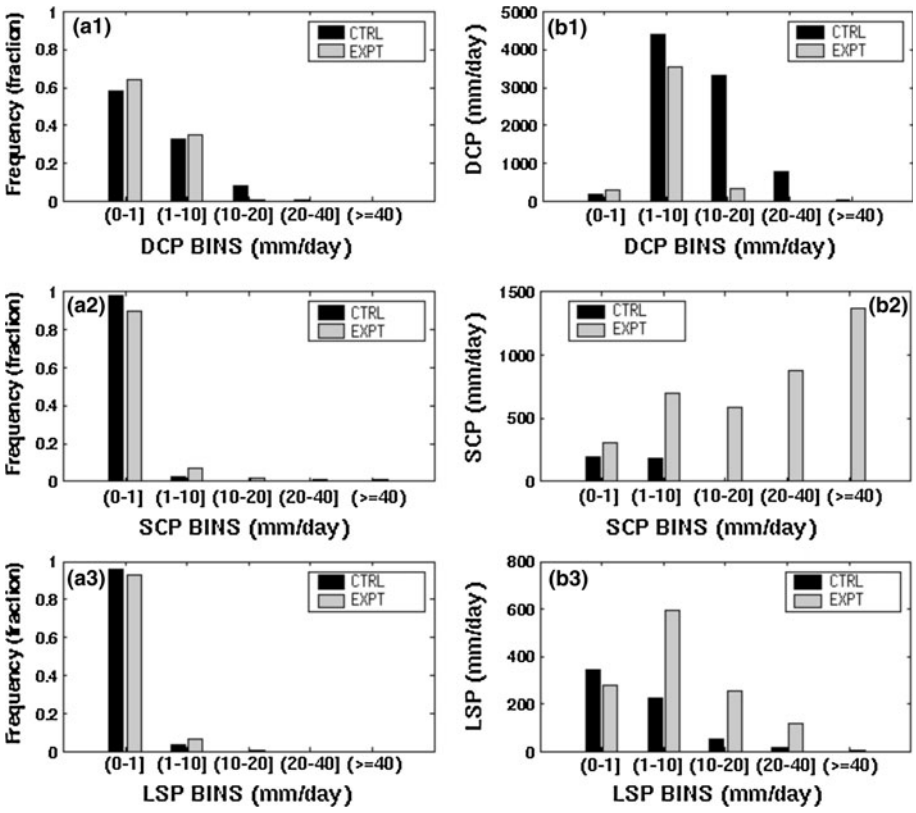

Fig. 19 **a1** Frequency distribution of daily deep convective precipitation rates in the tropics (0–360°E and 30°S–30°N) for 365 days, **b**1 amount of deep convective precipitation falling in each bin of precipitation rates, **a2** as in **a1**, but for shallow convective precipitation, **b2** as in **b1**, but for shallow convective precipitation, **a3** as in a1 but for large-scale precipitation, and **b3** as in **b1** but for large-scale precipitation

Acknowledgments Part of this work was carried out for Ph.D. thesis at Indian Institute of Science, during which the discussions with J. Srinivasan and S. Sahany are gratefully acknowledged. The author thanks Brian Mapes and Joe Tribbia for valuable interactions on related topics, and the reviewers for helpful comments. Michael Flanagan provided useful suggestions on the English language and helped improve its elucidation. Continuous support and encouragement of Ram Nair, Henry Tufo, and Mark Taylor is valuable, without which the manuscript would not have been on hand.

References

Betts AK, Miller MJ (1986) A new convective adjustment scheme. Part II: single column tests using GATE-wave, BOMEX, ATEX, and Arctic Airmass data sets. Q J R Meteorol Soc 112:693–710

Boville BA, Bretherton CS (2003) Heating and dissipation in the NCAR community atmosphere model. J Clim 16:3877–3887

Bretherton CS, Peters ME, Back LE (2004) Relationships between water vapor path and precipitation over the tropical oceans. J Clim 17:1517–1528

Collins WD et al. (2004) Description of the NCAR Community Atmosphere Model (CAM3). Tech. Rep. NCAR/TN-464+STR, National Center for Atmospheric Research, Boulder, pp 226

Collins WD et al (2006) The formulation and atmospheric simulation of the Community Atmosphere Model version 3 (CAM3). J Clim 19:2144–2161

Hack JJ (1994) Parameterization of moist convection in the National Center for Atmospheric Research Community Climate Model (CCM2). J Geophys Res 99(D3):5551–5568. doi:10.1029/93JD03478

Hayashi Y, Golder DG (1986) Tropical intraseasonal oscillation appearing in the GFDL general circulation model and FGGE data. Part I: Phase propagation. J Atmos Sci 43:3058–3067

Krishnamurti TN et al (1985) Divergent circulations on the 30 to 50 day time scale. J Atmos Sci 42:364–375

Lau KM, Peng L (1987) Origin of low-frequency (intraseasonal) oscillations in the tropical atmosphere. J Atmos Sci 44:950–972

Lau KM, Waliser DE (eds) (2005) Intraseasonal variability of the atmosphere–ocean climate system, Springer, Heidelberg, pp 474

Lau NC, Held IM, Neelin JD (1988) The Madden–Julian oscillations in an idealized general circulation model. J Atmos Sci 45:3810–3831

Lee JE, Pierrehumbert R, Swann A, Lintner BR (2009) Sensitivity of stable water isotopic values to convective parameterization schemes. Geophys Res Lett 36:L23801. doi:10.1029/2009GL040880

Lin JL, Mapes BE, Zhang M, Newman M (2004) Stratiform precipitation, vertical heating profiles, and the Madden- Julian Oscillation. J Atmos Sci 61:296–309

Locatelli JD, Hobbs PV (1974) Fall speeds and masses of solid precipitation particles. J Geophys Res 79:2185–2197

Lorant V, McFarlane NA, Scinocca JF (2006) Variability of precipitation intensity: sensitivity to treatment of moist convection in an RCM and a GCM. Clim Dyn 26:183–200

Mapes BE (2001) Empirical studies of unobservable parameters. In: ECMWF annual seminar course on physical parameterization

Mishra SK, Sahany S (2011a) Effects of time step size on the simulation of tropical climate in NCAR-CAM3. Clim Dyn 37:689–704. doi:10.1007/s00382-011-0994-4

Mishra SK, Sahany S (2011b) Sensitivity of Kelvin waves and Madden–Julian oscillation to convective downdrafts in the NCAR-CAM3. Atmo Sci Letts. doi:10.1002/asl.334

Mishra SK, Srinivasan J (2010) Sensitivity of the simulated precipitation to changes in convective relaxation time scale. Ann Geophys 28:1827–1846

Mishra SK, Srinivasan J, Nanjundiah RS (2008) The impact of time step on the intensity of ITCZ in aquaplanet GCM. Mon Weather Rev 136:4077–4091

Murakami T, Nakazawa T (1985) Tropical 45 day oscillations during the 1979 northern hemisphere summer. J Atmos Sci 42:1107–1122. doi:10.1175/1520-0469(1985)042<1107:TDODTN>2.0.CO;2

Nakazawa T (1988) Tropical super clusters within intraseasonal variations over the western Pacific. J Meteor Soc Japan 66:823–839

Neale RB, Hoskins BJ (2000) A standard test for AGCMs including their physical parametrizations. I: The proposal. Atmos Sci Lett 1:101–107

Park CK, Straus DM, Lau K-M (1990) An evaluation of the structure of tropical intraseasonal oscillations in three general circulation models. J Meteor Soc Japan 68:403–417

Rasch PJ, Kristjansson JE (1998) A comparison of the CCM3 model climate using diagnosed and predicted condensate parameterizations. J Clim 11:1587–1613

Rayner NA et al. (2003) Globally complete analyses of sea surface temperature, sea ice and night marine air temperature. J Geophys Res 108:(D14) 4407. doi:10.1029/2002JD002670

Sundqvist H (1988) Parameterization of condensation and associated clouds in models for weather prediction and general circulation simulation. In: Schlesinger ME (ed) Physically based modelling and simulation of climate and climatic change, vol 1. Kluwer Academic, Dordrecht, pp 433–461

Sui CH, Lau K-M (1989) Origin of low-frequency (intraseasonal) oscillations in the tropical atmosphere. Part II: Structure and propagation of mobile wave–CISK modes and their modification by lower boundary forcing. J Atmos Sci 46:37–56

Takahashi M (1987) A theory of the slow phase speed of the intraseasonal oscillation using wave–CISK. J Meteor Soc Japan 65:43–49.

Tokioka T, Yamazaki K, Kitoh A, Ose T (1988) The equatorial 30–60-day oscillation and the Arakawa–Schubert penetrative cumulus parameterization. J Meteor Soc Japan 66:883–901

Wheeler M, Kiladis GN (1999) Convectively coupled equatorial waves: analysis of clouds and temperature in the wavenumber–frequency domain. J Atmos Sci 56:374–399

Williamson DL (2008) Convergence of aqua-planet simulations with increasing resolution in the Community Atmospheric Model, Version 3. Tellus 60:848–862

Yanai M, Chen B, Tung W-W (2000) The Madden–Julian oscillation observed during the TOGA COARE IOP: global view. J Atmos Sci 57:2374–2396

Zhang GJ, McFarlane NA (1995) Sensitivity of climate simulations to the parameterization of cumulus convection in the CCGCM. Atmos Ocean 33:407–446